ISSN 1674-1056
http://cpb.iphy.ac.cn
http://iopscience.iop.org/cpb
中国物理 B
Chinese Physics
中国物理
Chinese Physics B

# Calculation and analysis of unbalanced magnetic pulls of different stator winding setups in static eccentric induction motor

Mingna Ma(马明娜), Yang Zhou(周洋), Xiaohua Bao(鲍晓华), Chunyu Wang(王春雨)

**Citation:**Chin. Phys. B . 2018, 27(8): 088401. **doi:** 10.1088/1674-1056/27/8/088401

Journal homepage: http://cpb.iphy.ac.cn; http://iopscience.iop.org/cpb

**What follows is a list of articles you may be interested in**

---

## Dynamical investigation and parameter stability region analysis of a flywheel energy storage system in charging mode

Zhang Wei-Ya, Li Yong-Li, Chang Xiao-Yong, Wang Nan
Chin. Phys. B . 2013, 22(9): 098401. **doi:** 10.1088/1674-1056/22/9/098401

---

# Calculation and analysis of unbalanced magnetic pulls of different stator winding setups in static eccentric induction motor*

Yang Zhou(周洋), Xiaohua Bao(鲍晓华)†, Mingna Ma(马明娜), and Chunyu Wang(王春雨)

*School of Electrical Engineering and Automation, Hefei University of Technology, Hefei* 230009, *China*

(Received 17 March 2018; revised manuscript received 17 May 2018; published online 10 July 2018)

In large-scale electric machines, unbalanced magnetic pull (UMP) caused by eccentricity usually results in stator-rotor rub, so it is necessary to investigate the amplitude and the influencing factors. This paper takes the squirrel-cage induction motor as an example. A magnetic loop model of an induction motor is established by an analytical method. The impact of stator winding setup (parallel branch and pole pairs) on each magnetomotive force (MMF) and unbalanced magnetic pull is analyzed. Using the finite element simulation method, the spatial and time distribution of flux density of the rotor outer circle under static eccentricity is obtained, and the unbalanced magnetic pull calculation caused by static eccentricity is completed. The conclusion of the influence of stator winding on the size of unbalanced magnetic pull provides reliable gist for motor noise and vibration analysis, and especially provides an important reference for large induction motor design.

**Keywords:** induction motor, static eccentricity, unbalanced magnetic pull, stator winding

**PACS:** 84.50.+d **DOI:** 10.1088/1674-1056/27/8/088401

## 1. Introduction

There are many reasons for the production of unbalanced magnetic pull: in general, the asymmetry of a magnetic circuit or electric circuit in the motor is the main cause. Non-overlapping of stator's and rotor's geometric centers is the regular factor for the production of unbalanced magnetic pull. Unbalanced magnetic pull problems are of particular concern in slender high-power motors, which include time-independent parts (the direction points to the smallest air gap) and time-dependent parts (twice power frequency fluctuations and slot harmonics).

In induction machines, the calculation of unbalanced magnetic pull becomes more complex in consideration of the rotor current. Domestic and foreign scholars have done much work on unbalanced magnetic pull. A simplified calculation model for unbalanced magnetic pull is established, which includes the analytic model[1] and finite element model.[2–4] These models are limited to two-dimensional eccentricity, and analytical models use a linear magnetic circuit. Dorrell, a British scholar, has done a lot of research on unbalanced magnetic pull. He introduced an unbalance magnetic pull calculation method,[5] and considered saturation and the axial variation of the air gap are taken into account.

In Refs. [6] and [7] a system for measuring unbalanced magnetic pull was proposed for a wound rotor motor. Tenhunen *et al.*[8] and Zhou *et al.*[9] used numerical methods to calculate the electromagnetic force in such eccentricities, and obtained results in good agreement with the measured values. Jiang *et al.*[10] studied the influence of the number of parallel branches of permanent magnet synchronous motor on average unbalanced magnetic pull under eccentricity. Dorrell *et al.*[11] applied conformal transformation and winding impedance coupling to the winding connection method, and studied the influence of the number of parallel branches in induction motor on average unbalanced magnetic pull force under eccentricity. Chong *et al.*[12] and Zhu *et al.*[13] analyzed the frequency characteristics of radial electromagnetic force. Bao *et al.*[14] made a summary of the study of eccentric unbalanced magnetic pull. Tang *et al.*[15] used theoretical derivation and numerical simulation to analyze the effects of radial air-gap eccentricity on unbalanced magnetic pull (UMP) of a turbo-generator's rotor and the rotor vibration characteristics. Doubly-fed induction machines[16] and wound rotor induction motors[17] are used to discuss UMP.

This paper is mainly based on the theoretical analysis of a magnetic circuit model of the motor and the finite element simulation. The influence of the stator winding arrangement (including the number of parallel branches and the number of stator poles) on the unbalanced magnetic pull of the eccentric induction motor is studied.

## 2. Mathematical model of the system

### 2.1. Eccentricity type

With the bearing aging, installation error, manufacturing error, and other reasons, mixed eccentricity phenomenon often inevitably appears in large-scale motor equipment. Mixed eccentricity is a combination of static and dynamic eccentric-

*Project supported by the National Natural Science Foundation of China (Grant Nos. 51677051 and 51377039) and the Fund from the Anhui Province Key Laboratory of Large-scale Submersible Electric Pump and Accoutrements.

†Corresponding author. E-mail: sukz@ustc.edu

© 2018 Chinese Physical Society and IOP Publishing Ltd 

ities. This paper mainly studies the characteristics of unbalanced magnetic pull caused by eccentricity and the factors that affect its size. Since one moment of dynamic eccentricity is equal to static eccentricity, therefore, for simplicity we only discuss the situation of static eccentricity and do not discuss dynamic and mixed situations.

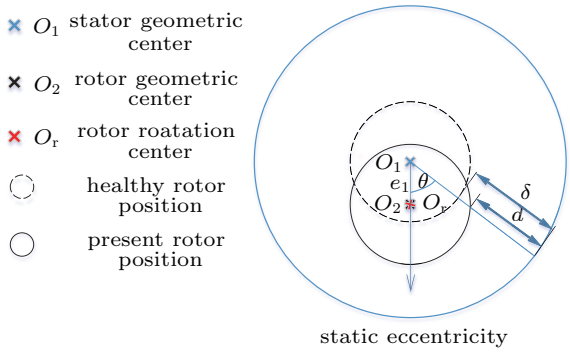



**Fig. 1.** (color online) Geometric locations of static eccentricity.

For static eccentricity, the geometric center of the rotor and the rotation center of the rotor overlap but there is a deviation between the geometric center of the stator and the rotation center of the rotor, as shown in Fig. 1. In the health condition of the motor, the stator geometric center $O_1$, the rotor geometric center $O_2$, and the rotor rotation center $O_r$ are all concentric. Since there is no deviation between the geometric center of the rotor and the rotation center of the rotor under static eccentricity, the air gap length between the inner circle of the stator and the outer circle of the rotor does not change as the rotor rotates but it changes in the circumferential direction.

In order to conveniently represent the air gap length expression, a relative polar coordinate system is set up in which the horizontal rightward direction is the positive direction of the polar axis and the counterclockwise direction is the positive direction of the polar angle. In practice, since the rotor outer radius $R_2$ is much larger than the normal air gap length $\delta$, ignoring a small amount $(\delta/R_2)^2$, the air gap length under static eccentricity is usually expressed as

$$d = \delta - e\cos(\theta + \theta_0), \tag{1}$$

where $e$ represents the offset of $O_1$ and $O_r$ under static eccentricity and $\theta_0$ is the polar angle where the air gap length is the smallest.

$$\xi = \frac{e}{\delta}. \tag{2}$$

For ease of description, eccentricity ratio $\xi$ is defined as Eq. (2).

### 2.2. Analysis of magnetic circuit of eccentricity

Eccentricity destroys the uniform distribution of air gap length between stator and rotor. For the rotating pole of an induction motor, figure 2 shows the magnetic circuit during actual operation. Its simplified magnetic circuit diagram is shown in Fig. 3. In the design of the motor, the magnetic reluctance of silicon steel sheet in the yellow zone in Fig. 3 is far less than the air gap reluctance at the maximum magnetic density moment. Under the condition of ensuring sufficient model accuracy, the loop flux expression is expressed as

$$\Phi = \frac{F_1 + F_2}{R_s + R_{a1} + R_{a2}} \approx \frac{F_m}{R_{a1} + R_{a2}}, \tag{3}$$

where the excitation MMF $F_m$ refers to the amplitude of the MMF of the largest loop in Fig. 2. $R_s$ is the magnetic reluctance of silicon steel sheet in the yellow zone in Fig. 3 and $R_{a1}$, $R_{a2}$ are the magnetic reluctance of air gaps.

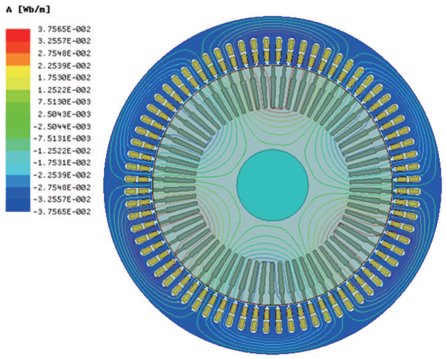


**Fig. 2.** (color online) Magnetic path of a 6-pole induction motor.

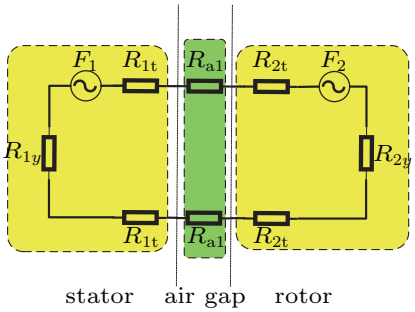



**Fig. 3.** (color online) Simplified magnetic circuit of one loop.

According to Eq. (3), we obtain the maximum air gap flux density as

$$B = \frac{\mu_0 F_m}{\delta_1 + \delta_2}. \tag{4}$$

Taking static eccentricity as an example, we substitute two air gap length values of the largest loop of one magnetic pole into Eq. (4). In Eq. (5), it can be seen that under the same magnitude of excitation MMF, fluctuation of effective air gap length in the denominator becomes larger along with rising pole numbers, and uneven space distribution of air gap flux density is intensified. When the pole pair is one, deterioration coefficient $K$ (6) becomes zero, i.e., there is no fluctuation of effective air gap length.

$$B = \frac{\mu_0 F_m}{\delta(1 - \xi\cos(\theta + \theta_0)) + \delta(1 - \xi\cos(\theta + \theta_0 + 2\pi/2p))}$$

$$= \frac{\mu_0 F_{\mathrm{m}}}{\delta(2-\xi\cos(\theta+\theta_0)-\xi\cos(\theta+\theta_0+2\pi/2p))}$$
$$= \frac{\mu_0 F_{\mathrm{m}}}{2\delta(1-\xi\cos(\pi/2p)\cos(\theta+\theta_0+\pi/2p))}, \quad (5)$$
$$K = \xi\cos(\pi/2p). \quad (6)$$

In addition, it should be noted that the MMF generated by different stator windings in the eccentric state does not completely change with the air gap length, resulting in asymmetry flux density distribution on the circumference. According to previous studies, the number of parallel branches of stator windings is an important factor affecting the distribution of magnetic flux density under eccentricity.

In order to accurately calculate the magnitude of the MMF at the circumferential position under eccentricity, the finite element software is used. The areas covering the stator pole and the rotor pole are drawn for calculation respectively. The deep color is the stator pole and the light color is the rotor pole as shown in Fig. 4. These areas are fixed and do not rotate with the rotor. For each of these areas, the following integral of the current density

$$F_p = \iint_S J_z \,\mathrm{d}S \quad (7)$$

can be used to obtain the MMF per pole at each location.

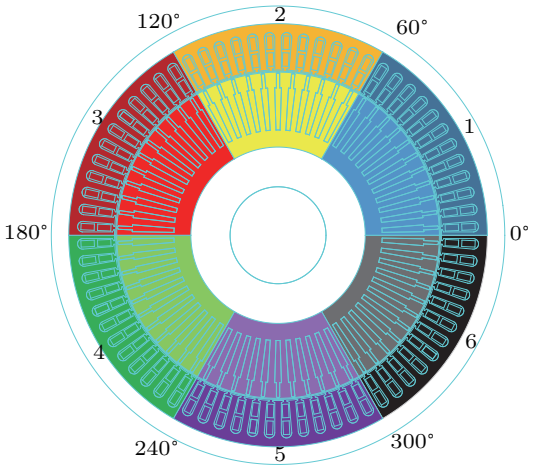



**Fig. 4.** (color online) Computing regions of stator poles and rotor poles.

### 2.3. Calculation method of unbalanced magnetic pull

According to the Maxwell tensor method, in order to make the force on the interface and other problems with ponderomotive force easy to be calculated, ponderomotive force (volume force) is often attributed to an equivalent group of tensions (area forces). The so-called equivalent means that the resultant force and moment acting on the magnetic substance of a given volume $V$ is exactly equal to the resultant force and moment of the tension on the surface $S$. $S$ is the surface of volume $V$. In the process of calculating the unbalanced magnetic pull, a circle close to the outer circle of the rotor is taken as the calculation curve in the two-dimensional (2D) model. The expression of magnetic tension is the same as in Eq. (8), where the flux density $B$ refers to the flux density perpendicular to the interface, called radial flux density acquired from the simulation model using the finite element package. Figure 5 shows a schematic diagram of unbalanced magnetic pull calculation. In this paper, the force in the direction of rotor deflection is only calculated. Equation (9) and the discrete magnetic tensions on the calculation circles are summed up to obtain the total unbalanced magnetic pull (10). Where $\mu_0$ is air permeability, $R_2$ is the outer radius of the rotor, $l$ is the axial length of the motor, $\alpha$ is the circumferential angle between the two points in Fig. 5, and $i$ is the number of the point on the calculation circle.

$$F = \frac{B^2}{2\mu_0} S, \quad (8)$$
$$F_{\mathrm{d}i} = \frac{1}{2\mu_0} B_i^2 l R_2 \alpha \cos[\alpha(i-1)], \quad (9)$$
$$F_{\mathrm{d}} = \sum_{i=1}^{720} F_{\mathrm{d}i}. \quad (10)$$

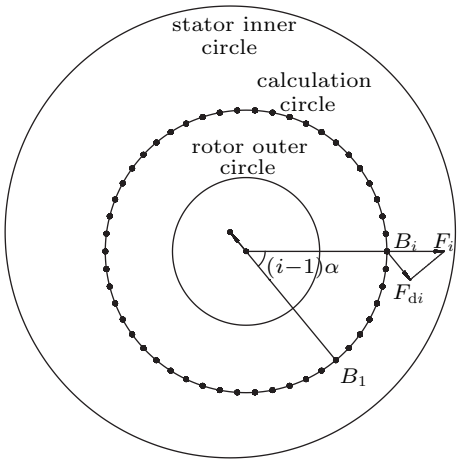



**Fig. 5.** Calculation of unbalanced magnetic pull.

## 3. Simulation analysis

With the help of finite element simulation, a 2D model of a 6-pole induction motor was built in this paper using the Maxwell 2D transient module. The motor parameters are shown in Table 1. In order to investigate the influence of parallel branch number on unbalanced magnetic pull under eccentricity, this paper focuses on the number of parallel branches at 1 and 6. For fair comparison, serial turns per phase are kept the same and copper weight used are the same as well. The specific parameters are shown in Table 2.

**Table 1.** Main parameters of healthy simulated induction motor.

| Parameters | Healthy simulated motor Motor |
|---|---|
| Rated power | 75 kW |
| Rated voltage | 380 V |
| Pole pair | 3 |
| Connection | △ |
| Rated frequency | 50 Hz |
| Number of stator slots $Z_1$ | 72 |
| Number of rotor slots $Z_2$ | 66 |
| Number of winding layers | 2 |
| Air gap length | 2.5 mm |

**Table 2.** Parameters of stator windings with different parallel branches.

| Number of parallel branches | $a = 1$ | $a = 6$ |
|---|---|---|
| Number of conductors per slot | 6 | 36 |
| Number of strands | 18 | 3 |
| Wire diameter | 1.4 mm | 1.4 mm |
| Pitch | 10 | 10 |
| Phase resistance | 0.0656677 Ω | 0.0656677 Ω |

### 3.1. Comparison of unbalanced magnetic pulls with parallel branches $a = 1$ and $a = 6$ under static eccentricity

The direct cause of inhomogeneous space distribution of flux density is the MMF. Figures 6 and 7 show the stator MMF, rotor MMF, and resultant MMF for different loads and different numbers of parallel branches under static eccentricity. The static eccentricity here refers to 60% static eccentricity, which is biased to 0 degree.

It can be seen from Fig. 6 that the rotor MMFs in each zone with $a = 1$ under no-load conditions have a big difference while the rotor MMF in each zone with $a = 6$ has a little difference. The increase in the number of parallel branches makes the stator MMF compensate for the rotor MMF to cope with the static eccentricity caused by the uneven spatial air gap, but the final resultant MMF has no significant difference. In Fig.7, the stator and rotor MMFs with $a = 1$ and $a = 6$ under full-load condition do not change much, but the harmonics of the resultant MMF are high and the stator slot harmonics are mostly obtained through decomposition. Since the change in the resultant MMF of each state is not obvious, in order to show the difference, the concept of a per-unit (P.U.) value is introduced. The P.U. value of the excitation MMF is based on the MMF per pole under health, and that of the air gap length is based on the air gap length under health. Figure 8 gives the P.U. values of flux density for each state, in which the excitation MMF is substituted for root mean square. The farther the curve value is from the health P.U. value 1, the greater the change in flux density. It can be clearly seen from this figure that the $a = 1$ curve has a greater change in flux density than the $a = 6$ curve, i.e., the unbalanced magnetic pull is greater; and the unbalanced magnetic pull becomes greater with load.

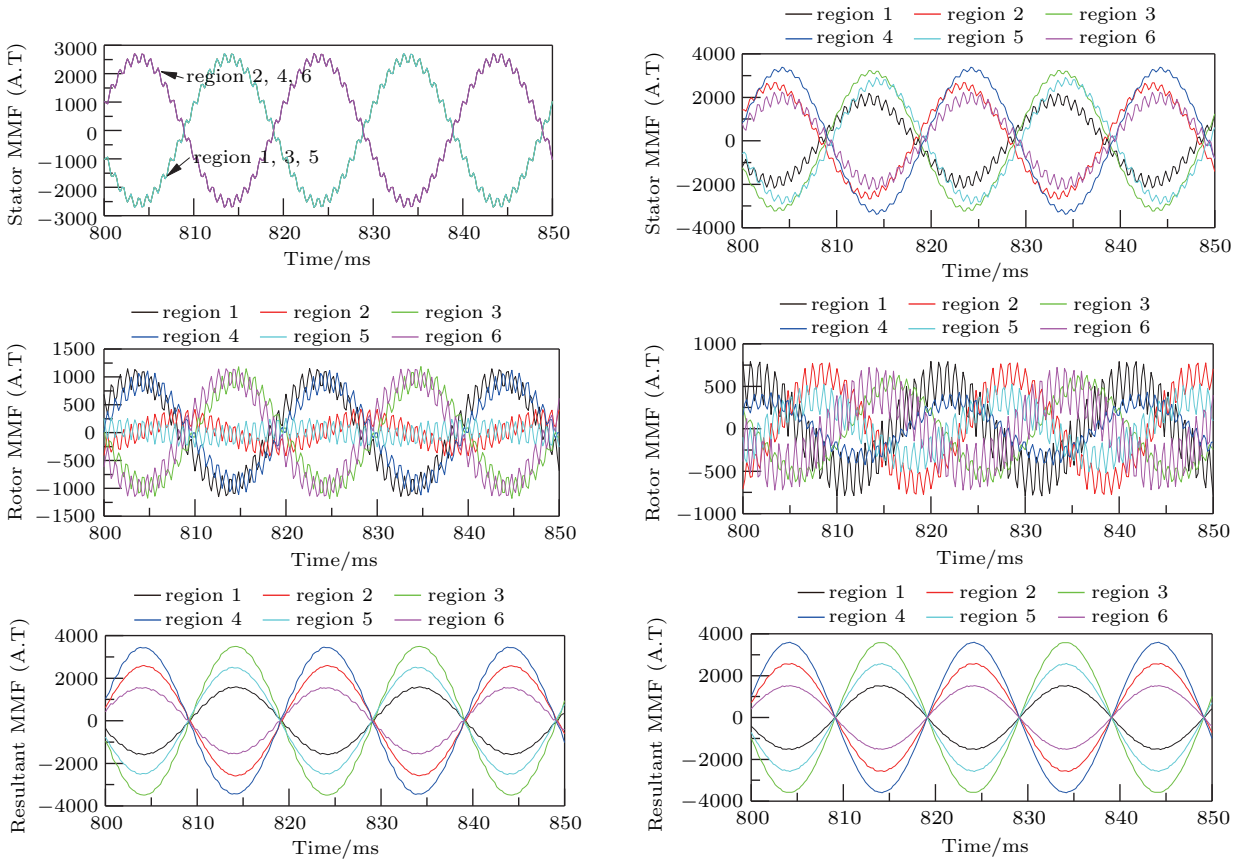



**Fig. 6.** (color online) MMFs of parallel branch $a = 1$ (left) and $a = 6$ (right) under static eccentricity (at no load).

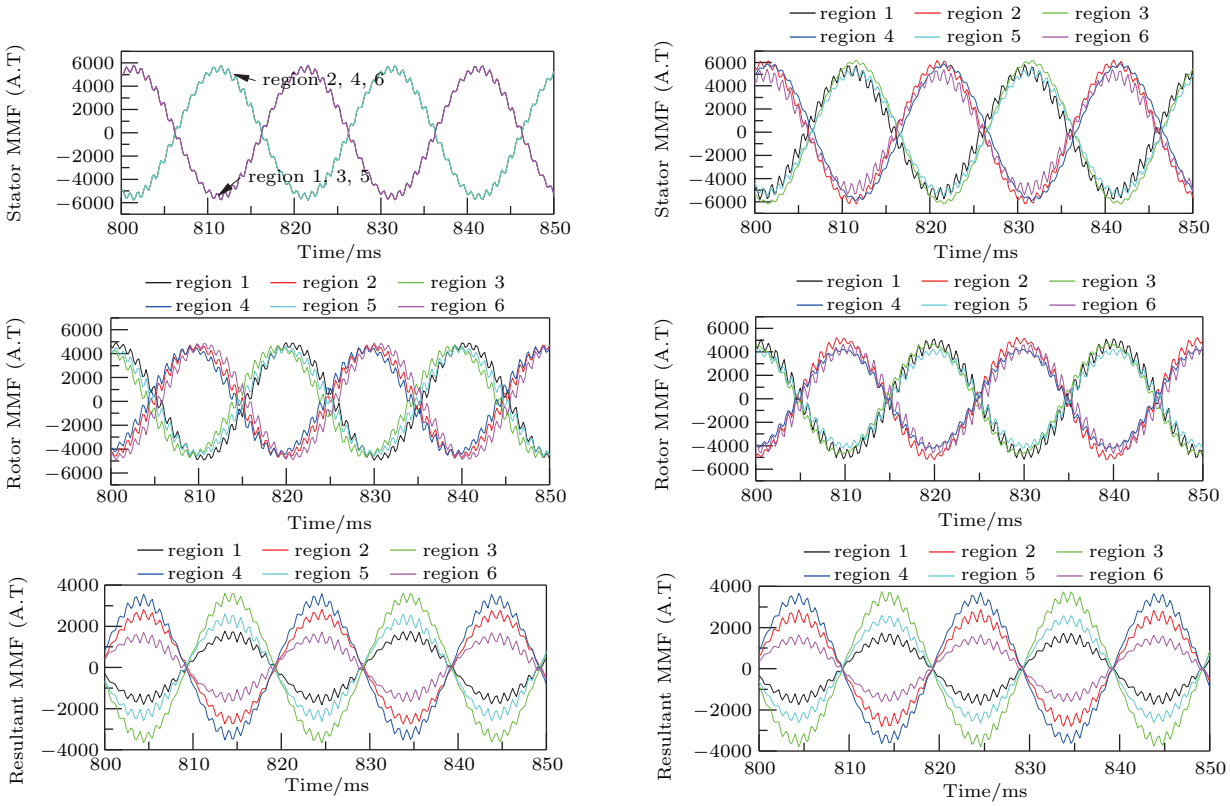



**Fig. 7.** (color online) MMFs of parallel branch $a = 1$ (left) and $a = 6$ (right) under static eccentricity (at full load).

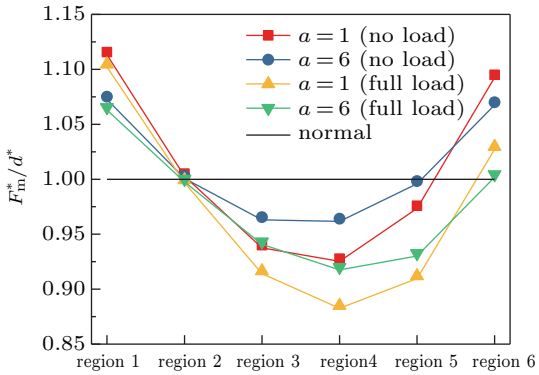



**Fig. 8.** (color online) Comparison of P.U. values at different loads and different parallel branches under the same static eccentricity.

According to the above-mentioned calculation method, the unbalanced magnetic pull in the deviation direction is calculated for different loads and different numbers of parallel branches under 0%, 20%, 40%, and 60% static eccentricity to verify the above-mentioned criteria. Figures 9–10 show the calculation result of UMPs under different situations. Figure 11 gives the main-frequency amplitudes of UMPs in Figs. 9–10. It can be seen from the figure that the 0-Hz UMP with $a = 1$ is much larger than that of $a = 6$ and full load increases the 0-Hz UMP. These results are consistent with the above conclusions. It has also been found that as the eccentricity ratio increases, the stator slot harmonic components (11) of the UMP increase. The amplitude of twice power frequency component generated after the square of flux density does not change much as the ratio of eccentricity increases, as shown in Fig. 11.

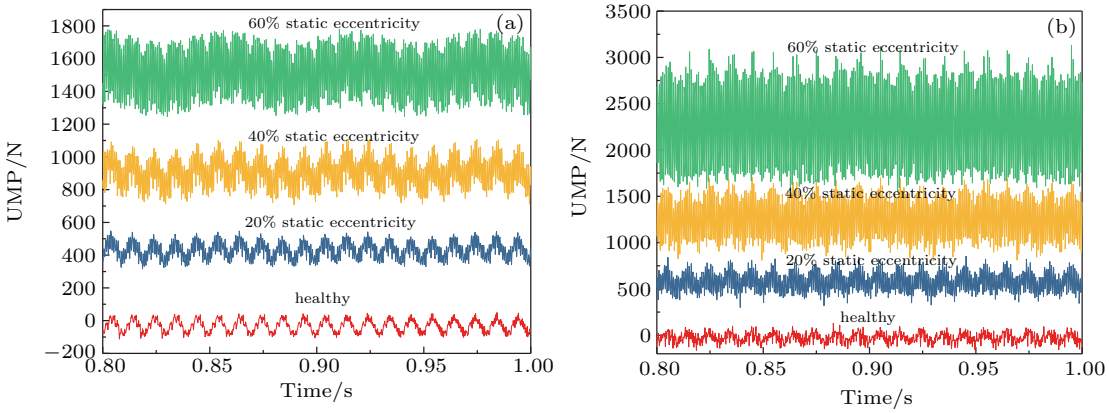



**Fig. 9.** (color online) UMPs of parallel branch $a = 1$ under static eccentricities at no load (a) and at full load (b).

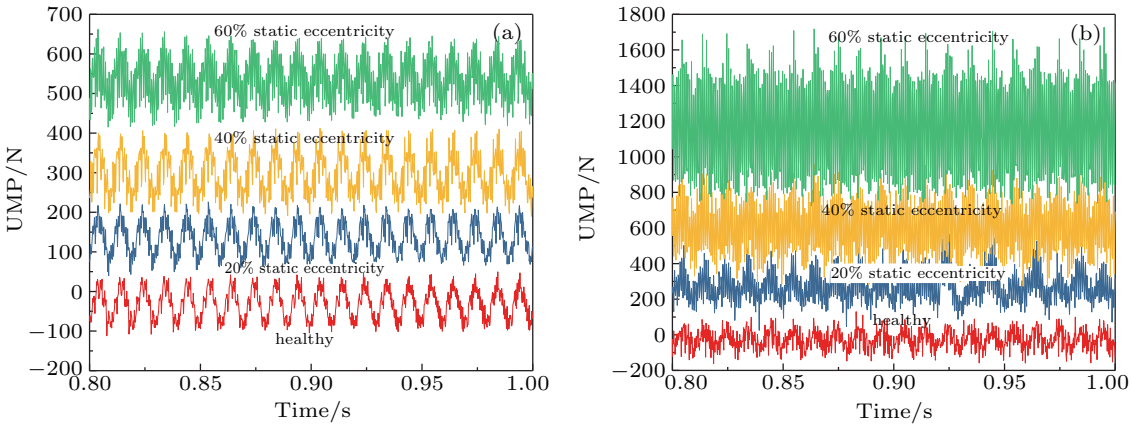



**Fig. 10.** (color online) UMPs of parallel branch $a = 6$ under static eccentricities at no load (a) and at full load (b).

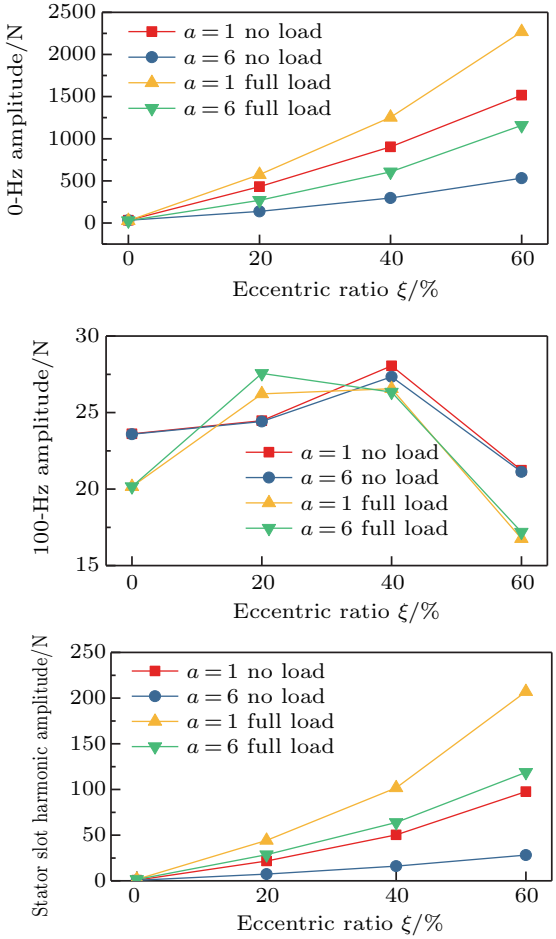



**Fig. 11.** (color online) Main-frequencies amplitude of UMP.

The slip $s$ at no load is 0.02%, and the slip $s$ at full load is 0.8%. The gravity of the rotor of the motor reaches 3200 N. Compared to the UMP growth rate of the eccentricity ratios at zero frequency, the amplitude of the stator slot harmonics increases much more slowly but only the high-frequency component (slot harmonics) makes sense on the vibration and noise of the motor. In addition, it should be noted that the direction of the force is from the position with large magnetic permeability to the position with small permeability. The direction of the unbalanced magnetic force calculated in this paper is the positive direction of the eccentric direction, i.e., the deviation is far from the center of the circle. The unbalanced magnetic pull acts as the result of deteriorating eccentricity.

$$f_s = \frac{Z_1 f}{p}(1-s). \tag{11}$$

### 3.2. Calculation of unbalanced magnetic pull with one pole pair under static eccentricity

According to Eq. (5), the degree of deterioration due to eccentricity is related to the number of pole pairs of the motor. In particular, when the number of pole pairs is 1, the maximum value of the air gap flux density does not change theoretically, and the deterioration of the inner magnetic circuit increases. This section changes the parameters of the simulation motor and designs a motor with a pole pair of 1 to calculate the unbalanced magnetic pull under static eccentricity. The model motor used in this section is basically the same as the parameters in Table 1, except that the stator winding and the stator outer diameter are changed. If the size of the motor is unchanged, the number of poles becomes smaller, and the number of magnetic circuits included in each pole region increases a lot. While the stator yoke width is not increased, the stator yoke is severely saturated. Therefore, the width of the stator yoke to a suitable value is increased. In order to ensure fair comparison, the air gap flux density of the design is basically the same as that of the 6-pole motor. The specific modification parameters are shown in Table 3.

**Table 3.** Comparative parameters of $p = 1$ and $p = 3$.

| | $p = 1$ | $p = 3$ |
|---|---|---|
| Number of conductors per slot | 2 | 6 |
| Number of strands | 54 | 18 |
| Wire diameter | 1.4 mm | 1.4 mm |
| Pitch | 30 | 10 |
| Stator outer diameter | 600 mm | 520 mm |

Figure 12 shows the calculation area for the stator and rotor poles of a two-pole motor. Figure 13 shows the results of

the calculation of the MMF under different loads. It can be seen from the figure that the change of the air gap has little effect on the MMF of the two-pole motor. Figure 14 shows the calculating result of the unbalanced magnetic pull and the amplitudes of the major frequencies of unbalanced magnetic pull under 60% static eccentricity. The average amount of unbalanced magnetic pull caused by the equivalent static eccentricity of a motor with a pole pair of 1 is much smaller than the amplitude of parallel branch $a = 1$ or 6 in a 6-pole motor as shown in Figs. 9–10, which is in accordance with Eq. (5).

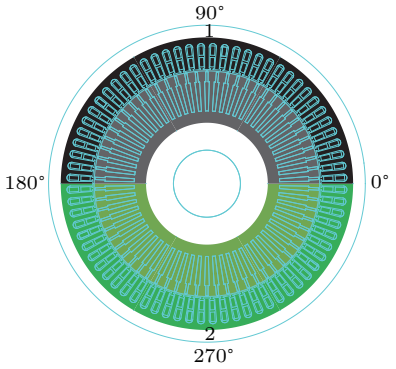



**Fig. 12.** (color online) Computing regions of stator poles and rotor poles ($p = 1$).

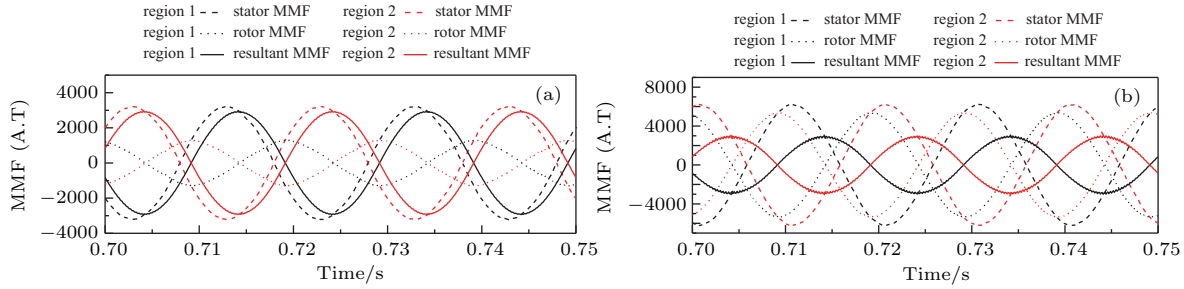



**Fig. 13.** (color online) Computing MMFs under 60% static eccentricity ($p = 1$) at no load (a) and at full load (b).

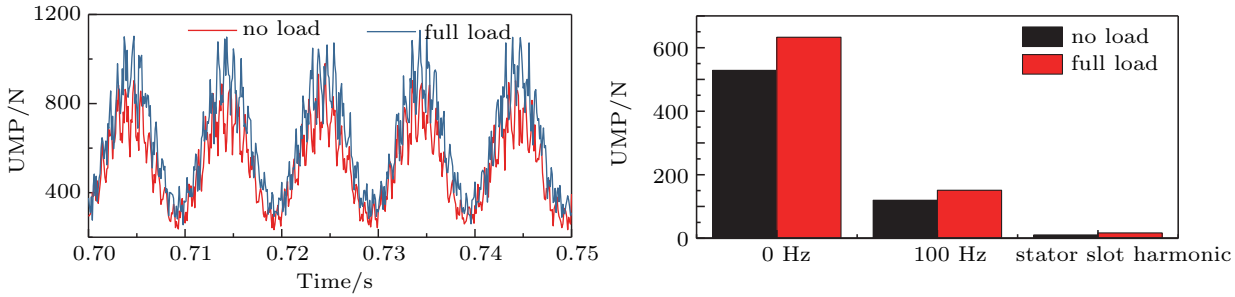



**Fig. 14.** (color online) UMPs of different loads and its spectrum under 60% static eccentricity ($p = 1$).

## 4. Conclusion and perspectives

This paper analyzes the influence of the number of parallel branches and the number of pole pairs on the unbalanced magnetic pull produced by the static eccentric induction motor. Through theoretical analysis and finite element simulation, the calculation and comparison of the unbalanced magnetic pull under each state are completed, and the following conclusions are made.

(i) According to the stator and rotor MMFs calculated above, spatial-arranged parallel branches of stator winding bear the variation of air gap length, which relieves the uneven distribution of air-gap flux density. So in the case of the same static eccentricity, the unbalanced magnetic pull of parallel branch $a = 6$ is much lower than that of parallel branch $a = 1$ under the same load. A larger load will aggravate UMP; furthermore, the UMP of parallel branch $a = 1$ at no load is even larger than that of parallel branch $a = 6$ at full load under the same eccentricity condition.

(ii) As the ratio of eccentricity intensifies, the amount of DC (which takes above 90% of total UMP) in the unbalanced magnetic pull increases quite linearly and fast. The component of twice power supply frequency does not change much along with eccentric ratio. The slot harmonic components climb fast, which is high frequency leading to the increase of electromagnetic noise.

(iii) In consideration of deterioration coefficient $K$ (6) introduced, while the number of pole pairs becomes larger, the ratio of eccentricity deterioration becomes greater and the unbalanced magnetic pull gets accordingly larger. Simulations verify that when the pole pair number is 1, the unbalanced magnetic pull is much smaller compared with $p = 3$ under the same size of motor. What is more, the influence of load on UMP is very small at $p = 1$.

## References

[1] Smith A C and Dorrell D G 1996 *IEE Proc. - Electric Power Appl.* **143** 193

[2] De Bortoli M J, Salon S J, Burow D W and Slavik C J 1993 *IEEE Trans. Magn.* **29** 1676
[3] Arkkio A, Antila M, Pokki K, Simon A and Lantto E 2000 *IEE Proc. - Electric Power Appl.* **147** 353
[4] Zhou Y, Bao X H, Di C and Wang L 2016 *IEEE Trans. Magn.* **52** 7
[5] Dorrell D G 2011 *IEEE Trans. Ind. Appl.* **47** 12
[6] Dorrell D G and Kayani O 2014 *IEEE Trans. Magn.* **50** 8103104
[7] Dorrell D G and Hsieh M F 2010 *IEEE Trans. Magn.* **46** 3029
[8] Tenhunen A 2011 *Proc. 4th International Symposium on Advanced Electromechanical Motion Systems — ELECTROMOTION*, 19–20 June, 2001, Bologna, Italy, p. 19
[9] Zhou L B and Ma Z Y 2002 *Large Electric Machine Hydraulic Turbine* **2** 26 (in Chinese)
[10] Jiang J W, Bilgin B, Sathyan A, Dadkhah H and Emadi A 2016 *IET Electric Power Appl.* **10** 526
[11] Dorrell D G and Smith A C 1994 *IEEE Trans. Energy Conversion* **9** 304
[12] Di C, Bao X H, Wang H F, Fang Y and Zhu Q L 2014 *Trans. Chin. Electrotechnical Soc.* **29** 138 (in Chinese)
[13] Zhu H F and Zhu C S 2013 *J. Mech. & Electr. Eng.* **30** 981 (in Chinese)
[14] Bao X H and Lü Q 2013 *Proc. CSEE* **33** 93 (in Chinese)
[15] Tang G J, Deng W Q and He Y L 2017 *J. Vib. Shock* **36** 15 (in Chinese)
[16] Moisson-Franckhauser N, Lug, T, Schwery A and Garbuio L 2017 15*th International Conference on Electrical Machines, Drives and Power Systems (ELMA)*, 2017, Sofia, pp. 383–388
[17] Dorrell D G, Salah A and Guo Y 2017 *IEEE Trans. Ind. Appl.* **53** 3